Science Advances

AAAS

advances.sciencemag.org/cgi/content/full/3/1/e1601536/DC1

Supplementary Materials for

The mechanics and design of a lightweight three-dimensional graphene assembly

Zhao Qin, Gang Seob Jung, Min Jeong Kang, Markus J. Buehler

Published 6 January 2017, *Sci. Adv.* **3**, e1601536 (2017)
DOI: 10.1126/sciadv.1601536

This PDF file includes:

Supplementary Materials

Supplementary Methods

Simulation of the forming of 3D graphene assembly

We apply an alternative *NPT-NVT* ensemble composed of 4 stages in each equilibration cycle to compress and fuse the graphene flakes to form the 3D architecture in our system as shown in Fig. 1C. Periodic conditions are applied to all the directions of the simulation box. The temperature and pressure of each simulation is controlled by a Nose-Hoover thermostat. For stage 1, we use the isothermal-isobaric (*NPT*) ensemble to keep the system at room temperature and linearly increase the targeting pressure p from 1 atm to p_1 = 1,000 atm for 50,000 dynamics steps as 25 ps (with 0.5 fs timestep); for stage 2 we use the canonical (*NVT*) ensemble to keep the volume constant by confining all the dimensions of the simulation box and increase the temperature T to T_1=2,000 K for 25 ps; for stage 3, we use *NVT* and keep both the volume and temperature constant for 25 ps; for stage 4, we keep the volume constant and reduce the temperature back to the ambient condition for the last 25 ps. By repeating this cycle, we manage to compress the graphene flake from its gas state to solid state, we calculate the number of covalent bonds by using the criterion of distance <1.6 Å for two carbon atoms and ensure its value and the density of the system converge before the end of each assembling simulation. It is noted to reach this connectivity we need to elevate the temperature to at least T_1 = 2,000 K, while future increment does not lead to larger N_{CC}. While the temperature plays a predominating role on N_{CC}, the density of the resulting structure is more dominated by p_1 within 1,000 atm, as shown in fig. S1.

Tensile and compression test on 3D graphene assembly

We deform the 3D graphene assembly in the quasi-static way. Periodic conditions are applied to all the directions of the simulation box. We first equilibrate the system in *NPT* ensemble with ambient condition (T = 300 K and p = 1 atm) and then deform the simulation box in a stepwise fashion for 1% uniaxial strain with p = 1 atm applied to the other two directions. Each strain increment is followed by an energy minimization and equilibration in *NVT* ensemble with T = 300 K.

The structure under compression force is mainly governed by the buckling of its constituting graphene walls as they are only of single atomic thickness, even with curved structure their bending stiffness is still lower than solid walls. The structure in tension is mainly governed by the stretching and rotation of the walls up to failure of the C-C covalent bonds. However, once the material is in tension, there is strong shrinkage with a Poisson ratio of 0.6. As a result, it is interesting to see that both the compression and tensile force reduce the volume and condense the material, making it ready for absorptions as shown in fig. S2.

All the measurement results of the mechanical properties, including Young's modulus, tensile and compression strength of the 3D graphene assembly are summarized in table S1 as a function of the material density.

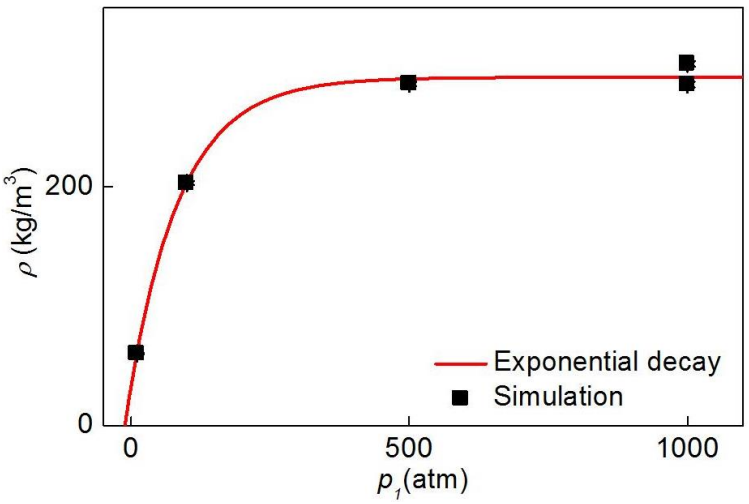

fig. S1. Material density of the graphene assembly as a function of elevated pressure. The different resulting density of the graphene assembly as a function of elevated pressure p_1 by keeping the elevate T_1 at 2,000 K. See Fig. 1 for the detailed synthesis protocol.

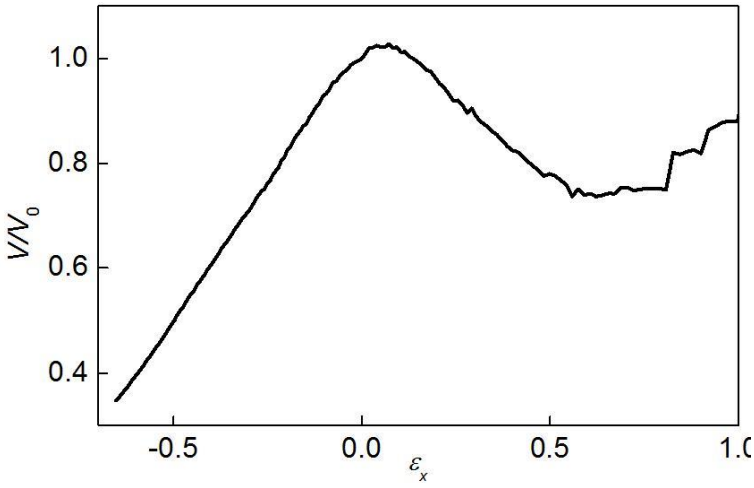

fig. S2. The total volume of the 3D graphene assembly as functions of the applied strain. The total volume of the 3D graphene assembly as functions of the applied strain during the compression ($\varepsilon_x<0$) and tensile ($\varepsilon_x>0$) tests.

table S1. Summary of the mechanical properties of different gyroid graphene structures. ρ_S = 2300 mg/cm^3, E_S = 1.02 TPa and σ_{TS} = 130 GPa correspond to the density, Young's modulus and tensile strength of graphene for its in-plane mechanics, which are used to normalize the property of graphene materials.

Model #	ρ (mg/cm^3)	E (GPa)	σ_T (GPa)	σ_C (GPa)
1	961.98	26.72	13.08	1.392
2	366.16	2.80	2.67	0.57
3	147.80	0.26	0.70	0.012
4	79.52	0.026	0.19	0.00007

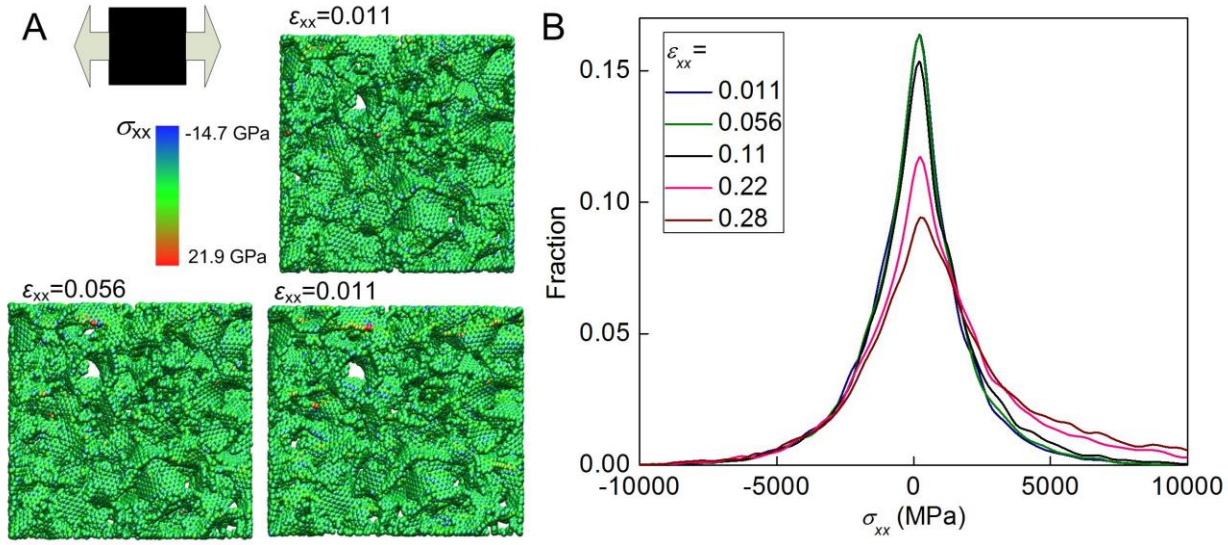

fig. S3. The atomic stress (σ_{xx}) distribution in the 3D graphene assembly under a tensile loading test. (**A)** Atomic stress (virial stress) is computed under different strain states (ε_{xx}) as noted. (**B)** The distribution of the atomic stress of all the atoms in the system under different strain states.

Modeling and simulation of the periodic gyroid structures

To understand the mechanical properties of the idealized 3D graphene we utilize the gyroid structure that has minimum surface area in a given volume, called minimal surface. Thus, the shape guarantees the minimum density under a given periodicity. The shape follows the equation

$$\sin\left(\frac{2\pi}{L}x\right)\cos\left(\frac{2\pi}{L}y\right)+\sin\left(\frac{2\pi}{L}y\right)\cos\left(\frac{2\pi}{L}z\right)+\sin\left(\frac{2\pi}{L}z\right)\cos\left(\frac{2\pi}{L}x\right)=0 \quad \text{(S1)}$$

where L is a parameter for dimension of a unit cell. In this study, we build five different atomistic models with different length constants (L: 3 ~ 20nm) by three steps. First, we introduce the external potential to Lennard-Jones particle system

$$E_{effect}=\sum E_{LJ}+\lambda\sum\left[\sin\left(\frac{2\pi}{L}x\right)\cos\left(\frac{2\pi}{L}y\right)+\sin\left(\frac{2\pi}{L}y\right)\cos\left(\frac{2\pi}{L}z\right)+\sin\left(\frac{2\pi}{L}z\right)\cos\left(\frac{2\pi}{L}x\right)\right]^2 \quad \text{(S2)}$$

to build a triangular template for the initial geometry. It is found that the shorter equilibrium distance of LJ potential $E_{LJ}=4\epsilon\left[\left(\frac{\sigma}{r_{ij}}\right)^{12}-\left(\frac{\sigma}{r_{ij}}\right)^{6}\right]$ than graphene bond (~1.42 Å) is better for the later process to refine geometry and ϵ has little effects on the geometry if strength of the external potential λ is strong enough to bind atoms on the surface. In our model, the parameters are set to $\epsilon=0.25$ kcal/mol, $\sigma=1.15$ Å, $r_{cut}=3.0$ Å and λ=460 kcal/mol. After we obtain the external potential term for each LJ potential, we apply this constraint on LJ particles having only less than 60kcal/mol. The value is carefully set to make sure one dense gyroid surface. If the value is too large, double layers of gyroid form, while a small value results in sparse geometry that requires more number of iterations in the next step. The initial geometry of LJ particles is chosen as fcc solid with 5.8 Å lattice constant as shown in fig. S3A. Then, the system is heated up to 1000K from 350K for 100ps. After the system is cooled down to 10K for another 100ps, we obtain the initial triangular geometry of the gyroid as shown in fig. S3B and C.

Second, we remove atoms based on the bond number for hexagonal geometry because the triangular geometry is not applicable for the refining algorithm. Figure S3D shows the schematic figure of the deleting algorithm. After obtaining the bond number of all atoms based on the distance criteria (here we set 2 Å), the atoms having more than 6 bonds are removed. After recalculation of the bond number, an atom having 6 bonds is selected (green dot) and deleted. In order to search next atoms to be deleted, we check all neighbors of green dot (one of them is blue

dot). Three candidates are easily found (white and red with number 2) by excluding the sharing atoms with green dot. For the hexagonal geometry, two white dots should be removed and one red dot should be remained. We distinguish them based on the bond number again: white dot shares two atoms with the green dot but red dot only share the blue dot with green dot. We remove all atoms under the conditions until there is no atom having six bonds. After removing atoms having 4 and 5 bonds, we obtain the hexagonal geometry for the next process as shown in fig. S3E.

Finally, we extend the previous the algorithm to generate polycrystalline graphene to refine the geometry obtained from the previous processes1. We add atoms based on the bond number and relaxed the structure with energy minimization and short MD runs. We utilize the modified potential based on Eq. (4) for gyroid graphene with the same parameters for the LJ potential. After removing atoms not satisfying three bonds, we add atoms to make hexagonal structures as shown in fig. 3SG. Iteratively, this process is repeated until there is no update anymore, and we obtain the final geometry of gyroid graphene structure as shown in fig. S3F. The quality of grain boundary is similar with the previous polycrystalline graphene models, which have mostly 5-7 rings and few 8 rings for the defects.

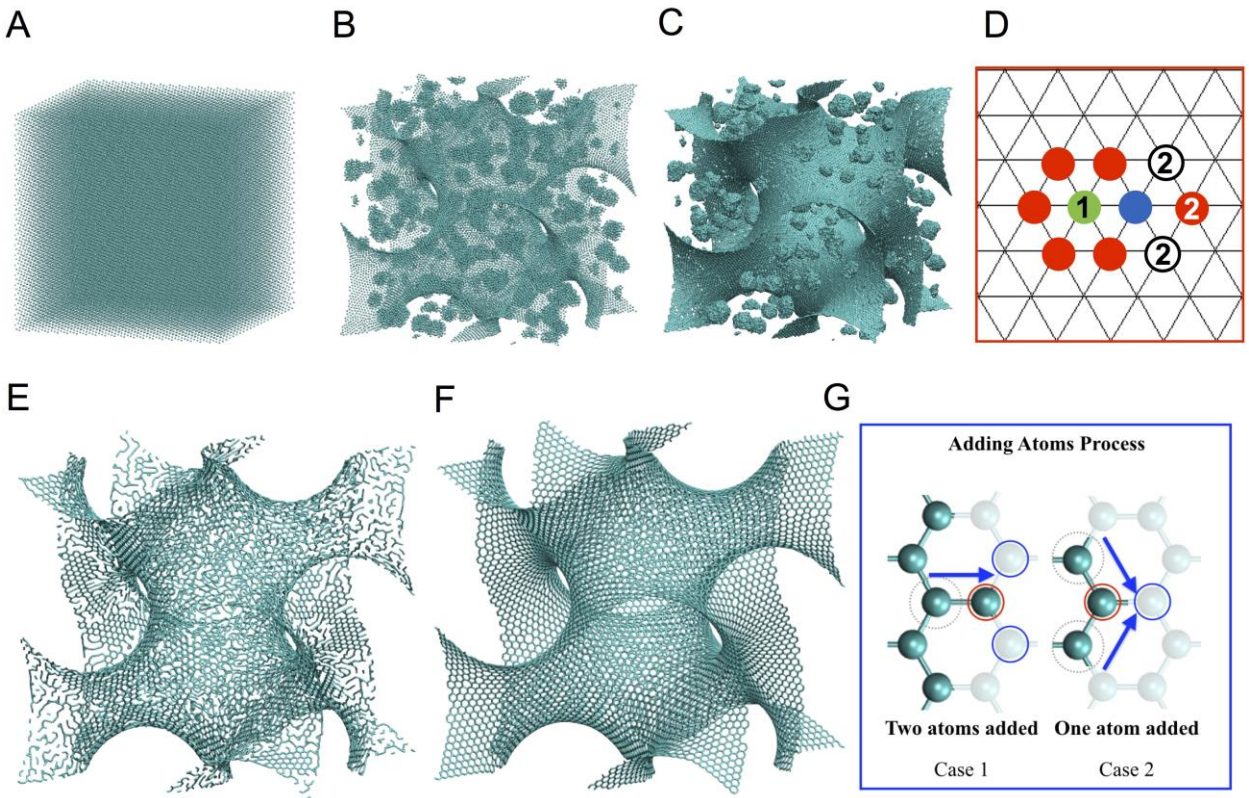

fig. S4. The processes of building a gyroid graphene structure from three steps. (**A-C)** generation of triangular gyroid structure with Lennard-Jones potential and the external potential, (**D-E)** modification from triangular to hexagonal gyroid based on our algorithm, **(F-G)** refinement of the geometry based on our iterative algorithm.

Mechanical properties of gyroid structures

First, we measure the elastic constants of five models. We relaxed the structures at 10K and 0 bar with Berendsen thermostat and barostat for 200 ps after the energy minimization. Then we calculate the elastic constant with 0.1% strain in all material directions. We perform the energy minimization after applying the strain and measure the stress. From the results of stress and strain, the elastic constants are obtained and Young's modulus is calculated from the constants.

Second, we obtain the stress-strain curves based on the tensile tests. After the structures are relaxed with the same conditions as described above, the systems are stretched in the x direction

with 0.5/ns strain rate and 1 fs time step for 1 ns under the plane strain condition. We test strain effects with 1/ns and 0.1/ns and realize there is no significant difference due to the strain rate. Figure S4A shows the stress-strain curves of the tensile test and the maximum stresses are selected as the critical stress for the scaling law in the main script. The snap-shots of detail deformation at different strain are shown in fig. S5A.

Finally, we obtain the stress-strain curves of the compressive tests. Figure S4B shows the obtained results. All relaxation preparing is the same as previous description and the compression strain rate is selected to 0.5/ns. The systems are compressed with only buckling mechanism without bond breakings. The deformation example of 10nm length constant (L) is shown in fig. S5B. Since there are common plateau regions without peak points of stress, we obtain the buckling stress by averaging the stress between 0.1 and 0.3 strains for the scaling law in the main script. All the analysis results are summarized in table S2.

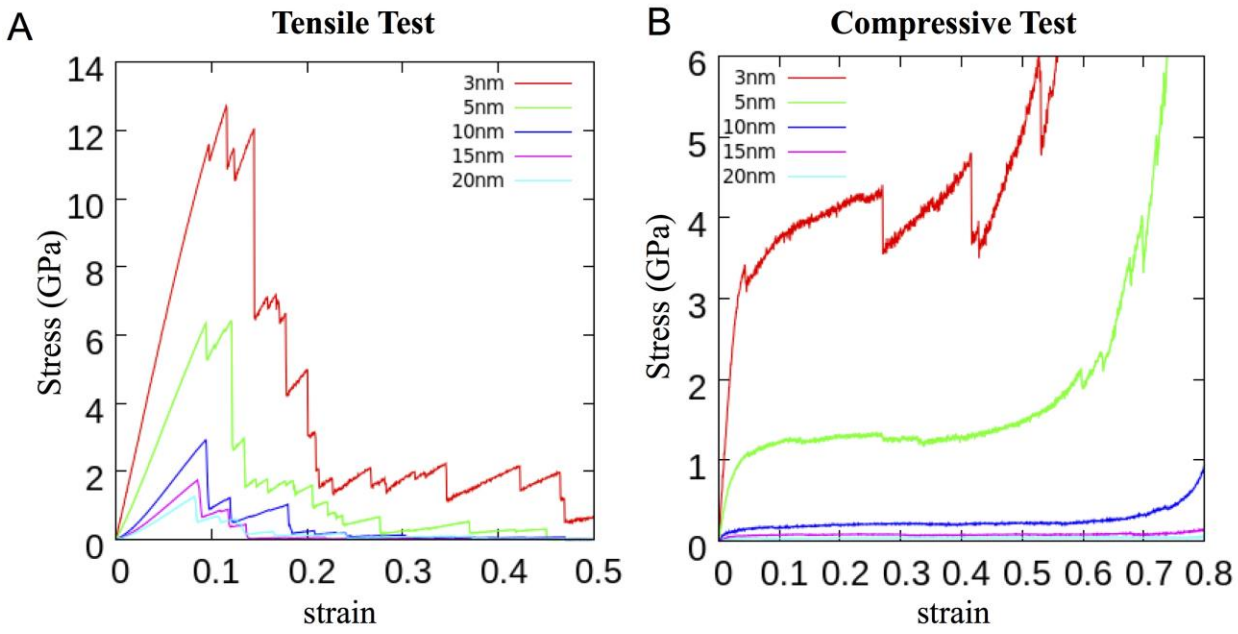

fig. S5. Stress-strain curves of tensile and compressive tests on gyroid graphene. Stress-Strain curves of gyroid graphene in (**A**) tensile and (**B**) compressive tests. We observe multiple breaking during the tensile loading and plateau region from 0.1 to 0.3 under the compressive loading.

table S2. Summary of the mechanical properties of different gyroid graphene structures. ρ_S = 2300 mg/cm^3, E_S = 1.02 TPa and σ_{TS} = 130 GPa corresponds to the density, Young's modulus and tensile strength of graphene for its in-plane mechanics, which are used to normalize the property of graphene materials.

L (nm)	ρ (mg/cm^3)	E (GPa)	σ_T (GPa)	σ_C (GPa)
3	814.79	81.09	12.7	4.02
5	510.13	35.43	6.4	1.27
10	253.87	12.54	2.9	0.198
15	169.35	9.03	1.7	0.081
20	126.77	5.79	1.3	0.038

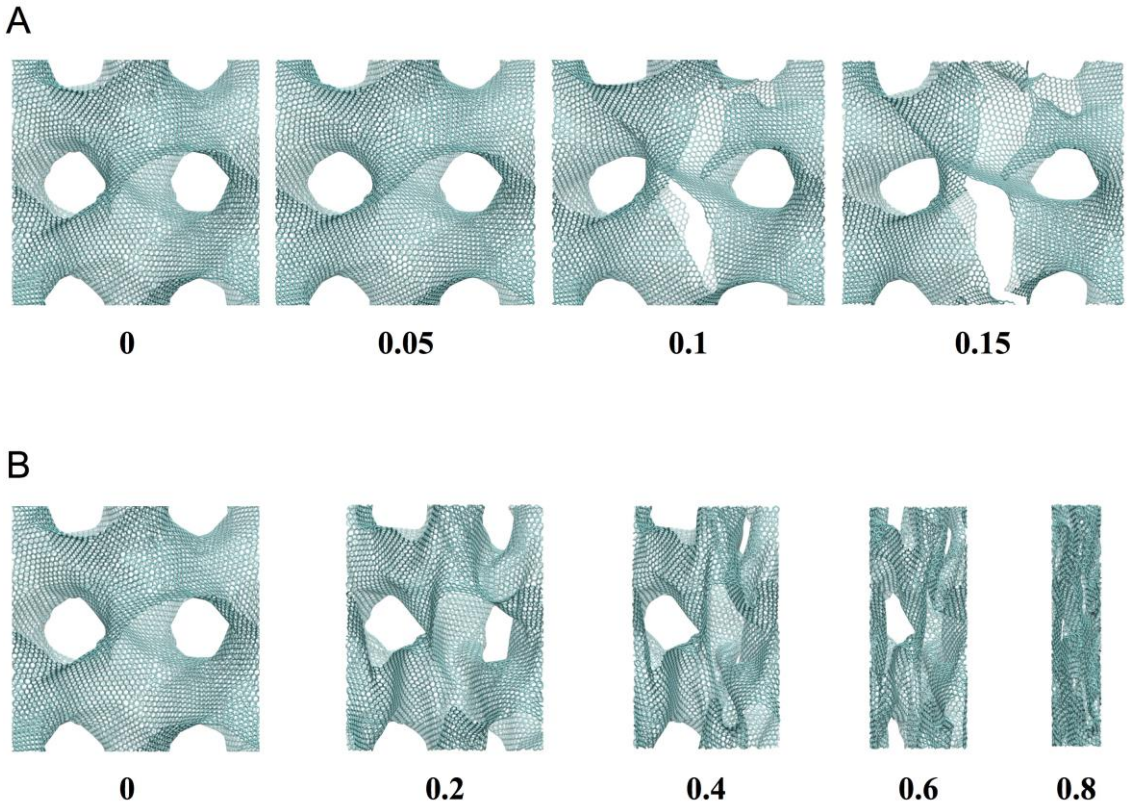

fig. S6. Snapshots of tensile and compressive tests with different strains on gyroid graphene. Snapshots of the deformation of gyroid graphene in (**A**) tensile and (**B)** compressive tests with different strain.

Mechanical tests on 3D printed gyroid samples

The tensile tests were carried out in room temperature with a standard tensile testing machine (MTS Corporation, Eden Prairie, Minnesota, USA, see fig. S7 for experimental set up and the design of the T-shape substrate). The strain-stress curves of gyroid samples of different density obtained from experiments are plotted in fig. S6 and the mechanical properties are summarized in table S3.

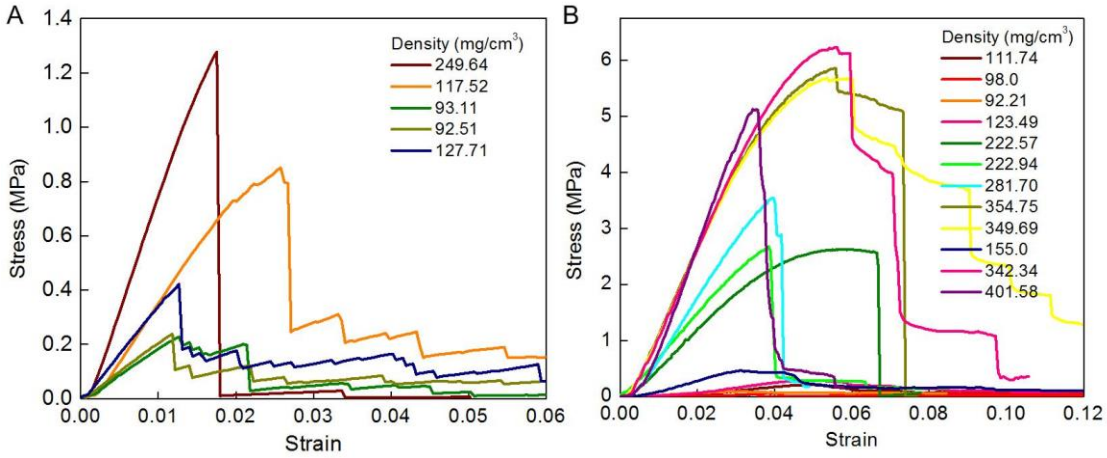

fig. S7. Stress-strain curves of tensile and compressive tests for 3D-printed gyroid samples. Stress-Strain curves of 3D printed gyroid samples in (**A**) tensile and (**B**) compressive tests.

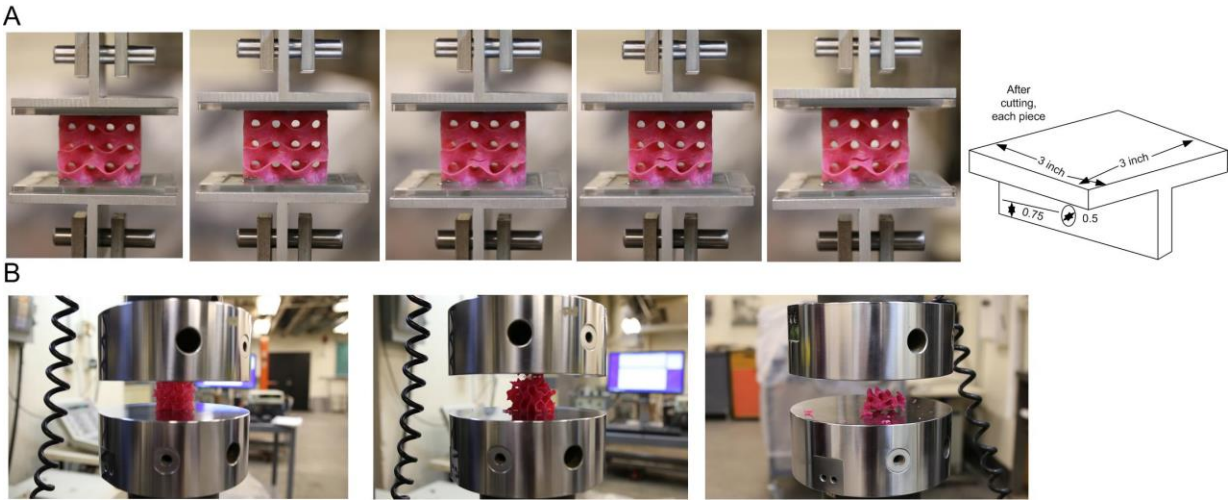

fig. S8. Experimental snapshots of the tensile and compressive tests on 3D-printed samples. Experimental snapshots of the (**A**) tensile and (**B**) compressive tests on 3D printed gyroid samples. The inserted schematic is the geometry of the T-shape aluminum substrate used for tensile tests on 3D printed samples.

table S3. Summary of the mechanical properties of different 3D graphene assemblies. It is noted that different from graphene, ρ_S = 1175 mg/cm^3, E_S = 2.45 GPa and σ_{Ts} = 50 MPa corresponds to the density, Young's modulus and tensile strength of the bulk material properties of polymer material for 3D printing.

Tensile tests			
Model #	**ρ (mg/cm^3)**	**E (MPa)**	**σ_T (MPa)**
1	249.64	85.58	1.28
2	117.53	43.35	0.85
3	93.12	20.52	0.23
4	92.52	21.83	0.24
5	127.71	36.60	0.42
Compression tests			
Model #	**ρ (mg/cm^3)**	**E (MPa)**	**σ_T (MPa)**
1	111.74	7.03	0.21
2	98.0	2.98	0.07
3	92.21	4.08	0.09
4	123.49	9.40	0.29
5	222.58	68.23	2.63
6	222.94	75.15	2.67
7	281.70	109.39	3.55
8	354.75	151.67	5.86
9	349.69	149.95	5.69
10	155.00	19.04	0.46
11	342.34	155.02	6.24
12	401.58	184.94	5.13